INTERNATIONAL JOURNAL OF
NUMERICAL ANALYSIS AND MODELING
Volume 7, Number 2, Pages 281–302

A NEW FINITE VOLUME METHOD FOR THE STOKES PROBLEMS

JUNPING WANG, YANQIU WANG, AND XIU YE

Abstract. A new finite volume method for solving the Stokes equations is developed in this paper. The finite volume method makes use of the BDM_1 mixed element in approximating the velocity unknown, and consequently, the finite volume solution features a full satisfaction of the divergence-free constraint as required for the exact solution. Optimal-order error estimates are established for the corresponding finite volume solutions in various Sobolev norms. Some preliminary numerical experiments are conducted and presented in the paper. In particular, a post-processing procedure was numerically investigated for the pressure approximation. The result shows a superconvergence for a local averaging post-processing method.

Key Words. finite volume methods, Stokes problems, discontinuous Galerkin method

1. Introduction

In scientific computing for science and engineering problems, finite volume methods are widely used and appreciated by users due to their local conservative properties for quantities which are of practical interest (e.g., mass or energy). Among many references, we would like to cite some which addresses theoretical issues such as stability and convergence [5, 6, 10, 11, 15, 16, 20, 21, 22, 8, 9, 10, 28, 29]. The goal of this paper is to investigate a finite volume method for the Stokes equations by using the well-known BDM elements [3] originally designed for solving second order elliptic problems. We intend to demonstrate how the BDM element can be employed in constructing finite volume methods for the model Stokes equations. The idea to be presented in the paper can be extended to problems of Stokes and Navier-Stokes type without any difficulty.

Mass conservation is a property that numerical schemes should sustain in computational fluid dynamics. This property is often characterized as an incompressibility constraint in the modeling equations. To sustain the mass conservation property for the Stokes equations, several finite element schemes have been developed to generate locally divergence-free solutions [12, 23]. In particular, a recent approach by using $H(\mathrm{div})$ conforming finite elements has been proposed and studied for a numerical approximation of incompressible fluid flow problems [13, 25, 26]. The main

1991 *Mathematics Subject Classification.* Primary, 65N15, 65N30, 76D07; Secondary, 35B45, 35J50 .

The research of Junping Wang was supported by the NSF IR/D program, while working at the Foundation. However, any opinion, finding, and conclusions or recommendations expressed in this material are those of the author and do not necessarily reflect the views of the National Science Foundation.

The research of Xiu Ye was supported in part by National Science Foundation Grant DMS-0813571.

advantage of using $H(\mathrm{div})$ conforming elements is that the discrete velocity field is exactly divergence-free. Another advantage of using $H(\mathrm{div})$ conforming elements is that the resulting linear or nonlinear algebraic systems can be easily decoupled between the velocity and the pressure unknowns, largely due to the availability of a computationally feasible divergence-free subspace for the velocity field. The purpose of this paper is to further explore the $H(\mathrm{div})$ conforming elements in a finite volume context.

Our model Stokes equations are defined on a two-dimensional domain Ω. The standard Dirichlet boundary condition is imposed on the velocity field. The Stokes problem seeks a velocity $\mathbf{u}$ and a pressure p such that

$$-\Delta \mathbf{u} + \nabla p = \mathbf{f} \quad \text{in } \Omega, \tag{1}$$

$$\nabla \cdot \mathbf{u} = 0 \quad \text{in } \Omega, \tag{2}$$

$$\mathbf{u} = \mathbf{g} \quad \text{on } \partial\Omega, \tag{3}$$

where the symbols Δ, ∇, and $\nabla\cdot$ denote the Laplacian, gradient, and divergence operators, respectively. $\mathbf{f}$ is the external volumetric force, and $\mathbf{g}$ is the velocity field on the boundary. For simplicity, we shall assume $\mathbf{g} = 0$ in the algorithmic description of the finite volume method. But the numerical experiments of Section 6 will be conducted for non-homogeneous data.

This paper is organized as follows. In Section 2, we introduce some notations that help us to give a technical presentation. In Section 3, a weak formulation is presented for the Stokes problem. Section 4 is dedicated to a presentation of a finite volume scheme by using the BDM element. In Section 5, we provide a theoretical justification for the finite volume scheme by establishing some error estimates in various norms. In addition to the standard H^1 and L^2 error estimates, we shall include an estimate for the pressure error in a negative norm, which ensures a certain superconvergence for the pressure when appropriate postprocessing methods are applied. In Section 6, a divergence-free finite volume formulation is discussed. Finally in Section 7, we present some numerical results that demonstrate the efficiency and accuracy of the new scheme.

2. Preliminaries and notations

We use standard notations for the Sobolev spaces $H^s(K)$ and their associated inner products $(\cdot,\cdot)_{s,K}$, norms $\|\cdot\|_{s,K}$, and semi-norms $|\cdot|_{s,K}$, $s \geq 0$ on a domain K. The space $H^0(K)$ coincides with $L^2(K)$, in which case the norm and inner product are denoted by $\|\cdot\|_K$ and $(\cdot,\cdot)_K$, respectively. The subscript K is suppressed when $K = \Omega$. Denote by $L_0^2(\Omega)$ the subspace of $L^2(\Omega)$ consisting of functions with mean value zero. Let $H(div, \Omega)$ be the space of all vector functions in $(L^2(\Omega))^2$ whose divergence is also in $L^2(\Omega)$, and $H_0(div, \Omega)$ be the space of all functions $\mathbf{v} \in H(div, \Omega)$ such that $\mathbf{v} \cdot \mathbf{n} = 0$ on $\partial\Omega$, where $\mathbf{n}$ is the unit outward normal vector.

Throughout the paper, we adopt the convention that a bold character in lower case stands for a vector. For simplicity, the Stokes problem (1)–(3) is assumed to have a full regularity of $\mathbf{u} \in (H^2(\Omega))^2$ and $p \in H^1(\Omega)$. In addition, we use $\lesssim$ ($\gtrsim$) to denote less than (greater than) or equal to up to a constant independence of the mesh size or other variables appeared in the inequality.

Let $\mathcal{T}_h$ be a quasi-uniform triangulation of Ω with characteristic mesh size h. Denote $\mathcal{E}_h$ to be the set of all edges in $\mathcal{T}_h$ and $\mathcal{E}_h^0 = \mathcal{E}_h \backslash \partial\Omega$ to be the set of all interior edges. Each triangle $T \in \mathcal{T}_h$ is further divided into three subtriangles by connecting the barycenter C to the vertices A_k, $k = 1, 2, 3$, as shown in Figure 1.

Denote the subtriangles by S_k, $k = 1, 2, 3$. Associated with each interior edge e, the two subtriangles which share the edge e form a quadrilateral. Similarly, each boundary edge is associated with one subtriangle. Define the dual partition $\mathcal{T}_h^*$ to be the union of these interior quadrilaterals and the border triangles.

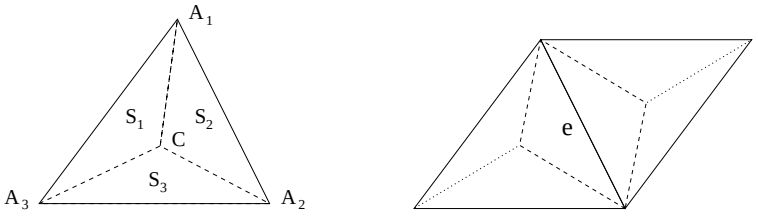

FIGURE 1. Subtriangles in T and the dual volume associated with interior edge e.

Let $P_k(T)$ be the set of all polynomials on T, with degree less than or equal to k. We use the lowest order Brezzi-Douglas-Marini element (BDM_1) to approximate the velocity. This element consists of piecewise linears on each triangle and the degrees of freedom are the zeroth and the first order momentum on each edge [3, 4]. Define the trial space V_h and the test space W_h for the velocity, respectively, by

$$V_h = \{\mathbf{v} \in H_0(div, \Omega) : \ \mathbf{v}|_T \in BDM_1(T), \ \ \forall T \in \mathcal{T}_h\},$$
$$W_h = \{\boldsymbol{\xi} \in L^2(\Omega)^2 : \ \boldsymbol{\xi}|_K \in P_0(K)^2, \ \ \forall K \in \mathcal{T}_h^*\}.$$

Notice that W_h is defined on the dual partition $\mathcal{T}_h^*$, which is a common feature of finite volume methods. Let the discrete space for pressure be defined by

$$Q_h = \{q \in L_0^2(\Omega) : \ q|_T \in P_0(T), \ \ \forall T \in \mathcal{T}_h\}.$$

For vectors $\mathbf{v}$ and $\mathbf{n}$, let $\mathbf{v} \otimes \mathbf{n}$ denote the matrix whose ijth component is $v_i n_j$ as in [13]. For two matrix valued variables σ and τ, we define $\sigma : \tau = \sum_{i,j=1}^{2} \sigma_{ij}\tau_{ij}$. Let e be an interior edge shared by two elements K_1 and K_2 in $\mathcal{T}_h$, and let $\mathbf{n}_1$ and $\mathbf{n}_2$ be unit normal vectors on e pointing exterior to K_1 and K_2, respectively. We define the average $\{\cdot\}$ and jump $[\cdot]$ on e for scalar q, vector $\mathbf{w}$ and matrix τ, respectively, by

$$\{q\} = \frac{1}{2}(q|_{\partial K_1} + q|_{\partial K_2}), \quad [q] = q|_{\partial K_1}\mathbf{n}_1 + q|_{\partial K_2}\mathbf{n}_2,$$
$$\{\mathbf{w}\} = \frac{1}{2}(\mathbf{w}|_{\partial K_1} + \mathbf{w}|_{\partial K_2}), \quad [\mathbf{w}] = \mathbf{w}|_{\partial K_1} \cdot \mathbf{n}_1 + \mathbf{w}|_{\partial K_2} \cdot \mathbf{n}_2,$$

and

$$\{\tau\} = \frac{1}{2}(\tau|_{\partial K_1} + \tau|_{\partial K_2}), \quad [\tau] = \tau|_{\partial K_1} \cdot \mathbf{n}_1 + \tau|_{\partial K_2} \cdot \mathbf{n}_2.$$

We also define a matrix valued jump $[\![\cdot]\!]$ for a vector $\mathbf{w}$ as $[\![\mathbf{w}]\!] = \mathbf{w}|_{\partial K_1} \otimes \mathbf{n}_1 + \mathbf{w}|_{\partial K_2} \otimes \mathbf{n}_2$ on e. If e is an edge on the boundary of Ω, define

$$\{q\} = q, \quad [\mathbf{w}] = \mathbf{w} \cdot \mathbf{n}, \quad \{\tau\} = \tau, \quad [\![\mathbf{w}]\!] = \mathbf{w} \otimes \mathbf{n}.$$

Let $V(h) = V_h + (H^2(\Omega) \cap H_0^1(\Omega))^2$ and $Q(h) = Q_h + (H^1(\Omega) \cap L_0^2(\Omega))$. Define a mapping $\gamma : V(h) \to W_h$ by

$$\gamma\mathbf{v}|_K = \frac{1}{h_e}\int_e \{\mathbf{v}\} ds \qquad \text{for all } K \in \mathcal{T}_h^*,$$

where $e \in \mathcal{E}_h$ is the edge associated with the dual volume K and h_e is the length of e.

Finally, we introduce three bilinear forms which will be used to describe a finite volume scheme in the coming section.

$$
\begin{aligned}
A_0(\mathbf{v},\mathbf{w}) &= -\sum_{K\in\mathcal{T}_h^*}\int_{\partial K}\frac{\partial \mathbf{v}}{\partial \mathbf{n}}\cdot(\gamma\mathbf{w})ds, \qquad B(\mathbf{v},q)=\sum_{T\in\mathcal{T}_h}\int_T \nabla\cdot\mathbf{v}q dx,\\
C(\mathbf{v},q) &= \sum_{K\in\mathcal{T}_h^*}\int_{\partial K} q(\gamma\mathbf{v})\cdot\mathbf{n}ds.
\end{aligned}
\tag{4}
$$

3. A weak formulation

The objective of this section is to derive a discrete weak formulation that will lead to a finite volume scheme for the Stokes problem. The main idea is to apply the conservative principle on each dual element $K \in \mathcal{T}_h^*$ and then seek for an approximate solution from the regular trial finite element space $V_h \times Q_h$. To this end, we multiply (1) and (2) by $\boldsymbol{\xi} \in W_h$ and $q \in Q_h$, respectively, and using integration by parts to obtain

$$
-\sum_{K\in\mathcal{T}_h^*}\int_{\partial K}\frac{\partial \mathbf{u}}{\partial \mathbf{n}}\cdot\boldsymbol{\xi}ds+\sum_{K\in\mathcal{T}_h^*}\int_{\partial K}p\boldsymbol{\xi}\cdot\mathbf{n}ds = (\mathbf{f},\ \boldsymbol{\xi}) \tag{5}
$$

$$
\sum_{T\in\mathcal{T}_h}\int_T \nabla\cdot\mathbf{u}q dx = 0, \tag{6}
$$

where $\mathbf{n}$ is the unit outward normal vector on ∂K. With the help of notation (4), it is easily seen that the solution $(\mathbf{u}, p)$ of (1)-(3) satisfies

$$
A_0(\mathbf{u},\mathbf{v})+C(\mathbf{v},p) = (\mathbf{f},\ \gamma\mathbf{v}) \qquad \text{for all } \mathbf{v}\in V(h), \tag{7}
$$

$$
B(\mathbf{u},q) = 0 \qquad \text{for all } q\in Q_h. \tag{8}
$$

When restricting all the functions in (7) and (8) into appropriate finite element spaces, the bilinear forms $A_0(\cdot,\cdot)$ and $C(\cdot,\cdot)$ can be represented in a way that resembles those from the standard finite element methods. Such a representation can shed light on a finite volume scheme that is stable and accurate. The rest of this section shall discuss various representations for the bilinear forms $A_0(\cdot,\cdot)$ and $C(\cdot,\cdot)$.

Denote by $(\cdot,\cdot)_{\mathcal{T}_h}$ the discrete L^2 inner-product as the summation of L^2 inner-products over all element $T \in \mathcal{T}_h$. The following two lemmas give equivalent representations for $A_0(\cdot,\cdot)$ and $C(\cdot,\cdot)$. Their proof will be given in Appendix A.

Lemma 1. *For $\mathbf{v},\mathbf{w}\in V(h)$, we have*

$$
\begin{aligned}
A_0(\mathbf{v},\mathbf{w}) =& (\nabla\mathbf{v},\nabla\mathbf{w})_{\mathcal{T}_h}-\sum_{e\in\mathcal{E}_h}\int_e\{\nabla\mathbf{v}\}:[\![\mathbf{w}]\!]ds\\
&+\sum_{e\in\mathcal{E}_h^0}\int_e[\nabla\mathbf{v}]\cdot\{\gamma\mathbf{w}-\mathbf{w}\}ds+(\Delta\mathbf{v},\mathbf{w}-\gamma\mathbf{w})_{\mathcal{T}_h}.
\end{aligned}
\tag{9}
$$

Furthermore, if $\mathbf{v}\in V_h$ and $\mathbf{w}\in V_h$, then

$$
A_0(\mathbf{v},\mathbf{w}) = (\nabla\mathbf{v},\nabla\mathbf{w})_{\mathcal{T}_h}-\sum_{e\in\mathcal{E}_h}\int_e\{\nabla\mathbf{v}\}:[\![\mathbf{w}]\!]ds. \tag{10}
$$

Lemma 2. *For $(\mathbf{v},q)\in V(h)\times Q(h)$, we have*

$$
C(\mathbf{v},q) = -(\nabla\cdot\mathbf{v},q)_{\mathcal{T}_h}+\sum_{T\in\mathcal{T}_h}\int_{\partial T}(\mathbf{v}-\gamma\mathbf{v})\cdot\mathbf{n}\,q\,ds+(\nabla q,\gamma\mathbf{v}-\mathbf{v})_{\mathcal{T}_h}. \tag{11}
$$

Furthermore, if $q \in Q_h$, then

$$C(\mathbf{v}, q) = -(\nabla \cdot \mathbf{v}, q)_{\mathcal{T}_h} = -B(\mathbf{v}, q). \tag{12}$$

4. Numerical schemes

In this section, we propose and study three discrete numerical schemes based on a stabilization of the weak formulation (7)–(8). To this end, we introduce a bilinear form as follows:

$$A_1(\mathbf{v}, \mathbf{w}) = A_0(\mathbf{v}, \mathbf{w}) + \alpha \sum_{e \in \mathcal{E}_h} \int_e h_e^{-1} [\![\mathbf{v}]\!] : [\![\mathbf{w}]\!] ds,$$

where $\alpha > 0$ is a parameter to be determined later. Note that the bilinear form $A_0(\cdot, \cdot)$ has the representation (10) when the arguments fall into the finite element space V_h. Thus, a skew-symmetric and a symmetric variation of $A_1(\cdot, \cdot)$ can be defined as follows:

$$\text{(skew-symmetric)} \quad A_2(\mathbf{v}, \mathbf{w}) = A_1(\mathbf{v}, \mathbf{w}) + \sum_{e \in \mathcal{E}_h} \int_e \{\nabla \mathbf{w}\} : [\![\mathbf{v}]\!] ds,$$

$$\text{(symmetric)} \quad A_3(\mathbf{v}, \mathbf{w}) = A_1(\mathbf{v}, \mathbf{w}) - \sum_{e \in \mathcal{E}_h} \int_e \{\nabla \mathbf{w}\} : [\![\mathbf{v}]\!] ds.$$

Notice that if $\mathbf{u}$ is smooth enough (e.g., $\mathbf{u} \in (H^{3/2+\varepsilon}(\Omega))^2$ for $\varepsilon > 0$), then

$$A_i(\mathbf{u}, \mathbf{v}) = A_0(\mathbf{u}, \mathbf{v}) \qquad \text{for all } \mathbf{v} \in V_h \text{ and } i = 1, 2, 3.$$

Define a bilinear form $D(r, q)$ as

$$D(r, q) = \beta \sum_{e \in \mathcal{E}_h^0} \int_e h_e [r][q] ds,$$

where $\beta \geq 0$.

The finite volume scheme seeks $(\mathbf{u}_h, p_h) \in V_h \times Q_h$ such that

$$A(\mathbf{u}_h, \mathbf{v}) + C(\mathbf{v}, p_h) = (\mathbf{f},\ \gamma \mathbf{v}) \qquad \text{for all } \mathbf{v} \in V_h, \tag{13}$$

$$B(\mathbf{u}_h, q) + D(p_h, q) = 0 \qquad \text{for all } q \in Q_h, \tag{14}$$

where $A(\cdot, \cdot)$ is one of $A_i(\cdot, \cdot)$, $i = 1, 2, 3$.

This finite volume method is consistent, i.e. the solution $(\mathbf{u}, p)$ of the Stokes equations (1)–(3) also satisfies the system:

$$A(\mathbf{u}, \mathbf{v}) + C(\mathbf{v}, p) = (\mathbf{f},\ \gamma \mathbf{v}) \qquad \text{for all } \mathbf{v} \in V_h, \tag{15}$$

$$B(\mathbf{u}, q) + D(p, q) = 0 \qquad \text{for all } q \in Q_h. \tag{16}$$

It can be shown that the discrete system (13)–(14) is well-posed. In fact, it follows from Lemma 2 that $C(\mathbf{v}, p_h) = -B(\mathbf{v}, p_h)$. In addition, it is well known that for BDM elements, the divergence operator from V_h to Q_h is onto. Hence by the mixed finite element theory [4, 24], one only needs to verify that $A(\cdot, \cdot)$ and $B(\cdot, \cdot)$ are continuous and $A(\cdot, \cdot)$ is coercive with respect to a suitably defined norm. Speaking

of norms, let us introduce the following norms and semi-norms on $V(h)$:

$$|\mathbf{v}|_{1,h}^2 = \sum_{T\in\mathcal{T}_h} |\mathbf{v}|_{1,T}^2, \qquad \|\mathbf{v}\|_e^2 = \int_e \mathbf{v}\cdot\mathbf{v}ds,$$
$$|||\mathbf{v}|||_1^2 = |\mathbf{v}|_{1,h}^2 + \sum_{e\in\mathcal{E}_h} h_e^{-1}\|[\![\mathbf{v}]\!]\|_e^2, \qquad |||\mathbf{v}|||^2 = |||\mathbf{v}|||_1^2 + \sum_{T\in\mathcal{T}_h} h_T^2|\mathbf{v}|_{2,T}^2,$$
$$|||[q]|||_0^2 = \beta\sum_{e\in\mathcal{E}_h^0} h_e\|[q]\|_e^2,$$

where h_T is the maximum edge length of T. The standard inverse inequality implies that

$$|||\mathbf{v}||| \lesssim |||\mathbf{v}|||_1 \qquad \forall \mathbf{v}\in V_h. \tag{17}$$

Let e be an edge of any triangle T. It is well known [1] that for any function $g\in H^1(T)$,

$$\|g\|_e^2 \lesssim \left(h_T^{-1}\|g\|_T^2 + h_T|g|_{1,T}^2\right). \tag{18}$$

The coercivity of the bilinear form $A(\cdot,\cdot)$ is given in two coming lemmas. The proof of these lemmas requires the following inequalities on the approximability of γ, whose proof will be given in Appendix B:

$$\|\mathbf{v}-\gamma\mathbf{v}\|_{\mathcal{T}_h} \lesssim h|||\mathbf{v}||| \qquad \text{for all } \mathbf{v}\in V(h), \tag{19}$$

$$\sum_{T\in\mathcal{T}_h}\int_{\partial T} |(\mathbf{v}-\gamma\mathbf{v})\cdot\mathbf{n}|^2\,ds \lesssim h|||\mathbf{v}|||^2 \qquad \text{for all } \mathbf{v}\in V(h). \tag{20}$$

Lemma 3. *For $\mathbf{v},\mathbf{w}\in V(h)$ and r, $q\in Q(h)$, we have*

$$A_i(\mathbf{v},\mathbf{w}) \lesssim |||\mathbf{v}|||\,|||\mathbf{w}||| \qquad \text{for } i=1,2,3, \tag{21}$$

$$C(\mathbf{v},q) \lesssim |||\mathbf{v}|||\left(\|q\|^2 + \sum_{T\in\mathcal{T}_h} h_T^2|q|_{1,T}^2\right)^{1/2}, \tag{22}$$

$$D(r,q) \lesssim |||[r]|||_0|||[q]|||_0 \lesssim |||[r]|||_0\left(\|q\|^2 + \sum_{T\in\mathcal{T}_h} h_T^2|q|_{1,T}^2\right)^{1/2}, \tag{23}$$

Furthermore, if $(\mathbf{v},q)\in V_h\times Q_h$, then

$$C(\mathbf{v},q) \lesssim |||\mathbf{v}|||\,\|q\|. \tag{24}$$

Proof. It follows from the Cauchy-Schwarz inequality and inequality (18) that

$$\left|\sum_{e\in\mathcal{E}_h}\int_e \{\nabla\mathbf{v}\} : [\![\mathbf{w}]\!]ds\right| \le \left(\sum_{e\in\mathcal{E}_h} h_e\|\{\nabla\mathbf{v}\}\|_e^2\right)^{1/2}\left(\sum_{e\in\mathcal{E}_h} h_e^{-1}\|[\![\mathbf{w}]\!]\|_e^2\right)^{1/2}$$
$$\lesssim \left(|\mathbf{v}|_{1,h}^2 + \sum_{T\in\mathcal{T}_h} h_T^2|\mathbf{v}|_{2,T}^2\right)^{1/2}\left(\sum_{e\in\mathcal{E}_h} h_e^{-1}\|[\![\mathbf{w}]\!]\|_e^2\right)^{1/2} \lesssim |||\mathbf{v}|||\,|||\mathbf{w}|||. \tag{25}$$

Similarly, by using the Cauchy-Schwarz inequality and inequalities (18), (19), it can be shown that

$$\left|\sum_{e\in\mathcal{E}_h^0}\int_e [\nabla\mathbf{v}]\cdot\{\gamma\mathbf{w}-\mathbf{w}\}ds\right| \lesssim |||\mathbf{v}|||\,|||\mathbf{w}|||.$$

Therefore, by using the representation (9) of Lemma 1, inequalities (18), (19), and the Cauchy-Schwarz inequality, we obtain

$$\begin{aligned}|A_1(\mathbf{v},\mathbf{w})| &\lesssim |\mathbf{v}|_{1,h}|\mathbf{w}|_{1,h} + |||\mathbf{v}|||\,|||\mathbf{w}||| + \|\Delta\mathbf{v}\|_{\mathcal{T}_h} h |||\mathbf{w}||| \\ &\quad + \alpha \left(\sum_{e\in\mathcal{E}_h} h_e^{-1}\|[\![\mathbf{v}]\!]\|_e^2\right)^{1/2} \left(\sum_{e\in\mathcal{E}_h} h_e^{-1}\|[\![\mathbf{w}]\!]\|_e^2\right)^{1/2} \\ &\lesssim |||\mathbf{v}|||\,|||\mathbf{w}|||.\end{aligned}$$

The same argument can be applied to handle the boundedness of $A_2(\cdot,\cdot)$ and $A_3(\cdot,\cdot)$.

As to the boundedness of the bilinear form $C(\cdot,\cdot)$, by using the representation (11) of Lemma 2, inequalities (18), (19) and (20), we have

$$\begin{aligned}|C(\mathbf{v},q)| &\le |\mathbf{v}|_{1,h}\|q\| + \left(h^{-1}\|q\|^2 + \sum_{T\in\mathcal{T}_h} h|q|_{1,T}^2\right)^{1/2} h^{1/2}|||\mathbf{v}||| + \|\nabla q\|_{\mathcal{T}_h} h |||\mathbf{v}||| \\ &\lesssim |||\mathbf{v}||| \left(\|q\|^2 + \sum_{T\in\mathcal{T}_h} h_T^2|q|_{1,T}^2\right)^{1/2}.\end{aligned}$$

This completes the proof of the boundedness estimate (22). (23) can be obtained similarly. The required inequality (24) follows immediately from the standard inverse inequality for finite element functions. □

Lemma 4. *For all $\mathbf{v}\in V_h$, we have the following coercivity results:*

$$A_i(\mathbf{v},\mathbf{v}) \gtrsim |||\mathbf{v}|||^2 \qquad \text{for } i=1,2,3, \tag{26}$$

provided that $\alpha>0$ for $i=2$ and sufficiently large values of α for $i=1,3$.

Proof. Using the representation (10) of Lemma 1, the inequality (25), and the standard inverse inequality for finite element functions, we obtain

$$\begin{aligned}A_1(\mathbf{v},\mathbf{v}) &= (\nabla\mathbf{v},\nabla\mathbf{v})_{\mathcal{T}_h} - \sum_{e\in\mathcal{E}_h}\int_e \{\nabla\mathbf{v}\} : [\![\mathbf{v}]\!]ds + \alpha\sum_{e\in\mathcal{E}_h}\int_e h_e^{-1}[\![\mathbf{v}]\!]^2 ds \\ &\ge |\mathbf{v}|_{1,h}^2 + \alpha\sum_{e\in\mathcal{E}_h} h_e^{-1}\|[\![\mathbf{v}]\!]\|_e^2 - C_0|\mathbf{v}|_{1,h}\left(\sum_{e\in\mathcal{E}_h} h_e^{-1}\|[\![\mathbf{v}]\!]\|_e^2\right)^{1/2} \\ &\gtrsim |||\mathbf{v}|||_1^2 \gtrsim |||\mathbf{v}|||^2,\end{aligned}$$

where C_0 is a positive constant related to the inverse inequality. Here, the last line is obtained by using the arithmetic-geometric mean inequality and by choosing α large enough.

The coercivity of $A_3(\cdot,\cdot)$ can be established in a similar manner. For $A_2(\cdot,\cdot)$, we have

$$\begin{aligned}A_2(\mathbf{v},\mathbf{v}) &= (\nabla\mathbf{v},\nabla\mathbf{v})_{\mathcal{T}_h} + \alpha\sum_{e\in\mathcal{E}_h}\int_e h_e^{-1}[\![\mathbf{v}]\!]^2 ds \\ &\ge min(1,\alpha)|||\mathbf{v}|||_1^2 \gtrsim min(1,\alpha)|||\mathbf{v}|||^2.\end{aligned}$$

□

The proof of Lemma 4 indicates that, for $i=1,3$, the value of α depends upon the constant in the inverse inequality. Therefore, the minimum value of α for which $A_1(\cdot,\cdot)$ is coercive is mesh dependent. Although this dependence is theoretically weak, it may still impose some inconvenience in practical computation because

the value of the parameter α has to be accurately estimated in order to have a mathematically well justified numerical scheme for the Stokes problem. To avoid the difficulty of selecting parameters, one is recommended to use the bilinear form $A_2(\cdot,\cdot)$ which is parameter insensitive.

5. Error estimates

In this section, we assume that α is properly selected so that $A(\cdot,\cdot)$ is coercive. To establish error estimates, we first need to verify the discrete inf-sup condition [4].

Lemma 5. *The bilinear form $B(\cdot,\cdot)$ satisfies the discrete inf-sup condition*

$$\sup_{\mathbf{v}\in V_h} \frac{B(\mathbf{v},q)}{|||\mathbf{v}|||} \gtrsim \|q\| \qquad \text{for all } q \in Q_h. \tag{27}$$

Proof. Let $\Pi_1 : (H_0^1(\Omega))^2 \to V_h$ be the local interpolation with respect to the degrees of freedom of the BDM_1 element. It has the following properties [4]:

$$\begin{aligned} B(\mathbf{v}-\Pi_1\mathbf{v},q) &= 0, && \text{for all } q \in Q_h \\ |\mathbf{v}-\Pi_1\mathbf{v}|_{s,T} &\lesssim h^{t-s}|\mathbf{v}|_{t,T}, && \text{for all } T \in \mathcal{T}_h,\ s=0,1, \text{ and } 1\le t\le 2. \end{aligned}$$

Hence it is not hard to see that

$$|||\mathbf{v}-\Pi_1\mathbf{v}|||_1 \lesssim \|\mathbf{v}\|_1 \qquad \text{for all } \mathbf{v} \in (H_0^1(\Omega))^2.$$

Then, it follows from $|||\mathbf{v}|||_1 = |\mathbf{v}|_1 \le \|\mathbf{v}\|_1$ and the triangle inequality that

$$|||\Pi_1\mathbf{v}|||_1 \lesssim \|\mathbf{v}\|_1. \tag{28}$$

To verify (27), we first use the operator Π_1 to obtain

$$\sup_{\mathbf{v}\in V_h} \frac{B(\mathbf{v},q)}{|||\mathbf{v}|||} \ge \sup_{\mathbf{v}\in (H_0^1(\Omega))^2} \frac{B(\Pi_1\mathbf{v},q)}{|||\Pi_1\mathbf{v}|||} = \sup_{\mathbf{v}\in (H_0^1(\Omega))^2} \frac{B(\mathbf{v},q)}{|||\Pi_1\mathbf{v}|||}. \tag{29}$$

Observe that by using (28), and (17), we have for all $\mathbf{v} \in (H_0^1(\Omega))^2$

$$|||\Pi_1\mathbf{v}||| \lesssim |||\Pi_1\mathbf{v}|||_1 \lesssim \|\mathbf{v}\|_1. \tag{30}$$

Thus, substituting (30) into inequality (29) gives

$$\sup_{\mathbf{v}\in V_h} \frac{B(\mathbf{v},q)}{|||\mathbf{v}|||} \gtrsim \sup_{\mathbf{v}\in (H_0^1(\Omega))^2} \frac{B(\mathbf{v},q)}{\|\mathbf{v}\|_1} \gtrsim \|q\|,$$

where we have used the *inf-sup* condition for the continuous case [4, 19]. □

5.1. Error estimate in $H^1 \times L^2$. We first establish an optimal-order error estimate for the velocity in $|||\cdot|||$-norm and for the pressure in the L^2-norm. Observe that the solution of the Stokes problem (1)–(3) satisfies equations (15)–(16) and the discrete solution satisfies (13)–(14). Thus, the error estimate in $H^1 \times L^2$ can be derived by following a routine procedure in the theory for mixed finite element methods [4].

Theorem 1. *Let $(\mathbf{u}_h, p_h) \in V_h \times Q_h$ be the solution of* (13)–(14) *and $(\mathbf{u}, p) \in (H^2(\Omega)\cap H_0^1(\Omega))^2 \times (L_0^2(\Omega)\cap H^1(\Omega))$ be the solution of* (1)–(3)*. Then, one has*

$$|||\mathbf{u}-\mathbf{u}_h||| + \|p-p_h\| \lesssim |||\mathbf{u}-\Pi_1\mathbf{u}||| + \|p-\Pi_2 p\| + h\|p\|_1. \tag{31}$$

Proof. Let Π_1 be defined as in the proof of Lemma 5, and Π_2 be the L^2 projection from $L_0^2(\Omega)$ to the finite element space Q_h. Let

$$\epsilon_h = \mathbf{u}_h - \Pi_1 \mathbf{u}, \qquad \eta_h = p_h - \Pi_2 p \tag{32}$$

be the error between the finite volume solution $(\mathbf{u}_h, p_h)$ and the projection $(\Pi_1\mathbf{u}, \Pi_2 p)$ of the exact solution. Denote by

$$\epsilon = \mathbf{u} - \Pi_1 \mathbf{u}, \qquad \eta = p - \Pi_2 p \tag{33}$$

the error between the exact solution $(\mathbf{u}, p)$ and its projection. Subtracting (13) and (14) from (15) and (16), respectively, we have

$$A(\epsilon_h, \mathbf{v}) + C(\mathbf{v}, \eta_h) = A(\epsilon, \mathbf{v}) + C(\mathbf{v}, \eta), \tag{34}$$

$$B(\epsilon_h, q) + D(\eta_h, q) = B(\epsilon, q) + D(\eta, q), \tag{35}$$

for all $\mathbf{v} \in V_h$ and $q \in Q_h$.

By setting $\mathbf{v} = \epsilon_h$ in (34) and $q = \eta_h$ in (35), and using Lemma 2 and the fact $B(\epsilon, \eta_h) = 0$, the sum of (34) and (35) gives

$$A(\epsilon_h, \epsilon_h) + D(\eta_h, \eta_h) = A(\epsilon, \epsilon_h) + C(\epsilon_h, \eta) + D(\eta, \eta_h). \tag{36}$$

Thus, it follows from the coercivity (26) and the boundedness (21), (22), (23) that

$$|||\epsilon_h|||^2 + |||[\eta_h]|||_0^2 \lesssim |||\epsilon||| |||\epsilon_h||| + \left(\|\eta\|^2 + \sum_{T \in \mathcal{T}_h} h_T^2 |\eta|_{1,T}^2 \right)^{1/2} (|||\epsilon_h||| + |||[\eta_h]|||_0),$$

which implies that

$$|||\epsilon_h||| + |||[\eta_h]|||_0 \lesssim |||\epsilon||| + \|\eta\| + \left(\sum_{T \in \mathcal{T}_h} h_T^2 |\eta|_{1,T}^2 \right)^{1/2}.$$

The above estimate, combined with the triangle inequality and the well-known H^1 stability of the L^2 projection Π_2, gives

$$|||\mathbf{u} - \mathbf{u}_h||| + |||[p - p_h]|||_0 \lesssim |||\mathbf{u} - \Pi_1 \mathbf{u}||| + \|p - \Pi_2 p\| + h\|p\|_1, \tag{37}$$

which completes the estimate for the velocity approximation.

As to the error for the pressure approximation, it follows from the discrete inf-sup condition (27), the representation (12) of Lemma 2, inequalities (21), (22), and (37) that

$$\begin{aligned}
\|p_h - \Pi_2 p\| &\lesssim \sup_{\mathbf{v} \in V_h} \frac{B(\mathbf{v}, p_h - \Pi_2 p)}{|||\mathbf{v}|||} = \sup_{\mathbf{v} \in V_h} \frac{C(\mathbf{v}, \Pi_2 p - p_h)}{|||\mathbf{v}|||} \\
&= \sup_{\mathbf{v} \in V_h} \frac{A(\mathbf{u}_h - \mathbf{u}, \mathbf{v}) + C(\mathbf{v}, p - \Pi_2 p)}{|||\mathbf{v}|||} \\
&\lesssim |||\mathbf{u} - \mathbf{u}_h||| + \|p - \Pi_2 p\| + \left(\sum_{T \in \mathcal{T}_h} h_T^2 |p - \Pi_2 p|_{1,T}^2 \right)^{1/2} \\
&\lesssim |||\mathbf{u} - \Pi_1 \mathbf{u}||| + \|p - \Pi_2 p\| + h\|p\|_1.
\end{aligned}$$

Then the desired estimate (31) follows by using the standard triangle inequality. □

5.2. An L^2 error estimate for the velocity approximation. We first introduce a dual problem: find $(\mathbf{w}, \lambda) \in H_0^1(\Omega)^2 \times L_0^2(\Omega)$ satisfying

$$-\Delta \mathbf{w} + \nabla \lambda = \mathbf{u} - \mathbf{u}_h \qquad \text{in } \Omega, \tag{38}$$

$$\nabla \cdot \mathbf{w} = 0 \qquad \text{in } \Omega, \tag{39}$$

$$\mathbf{w} = 0 \qquad \text{on } \partial\Omega. \tag{40}$$

As assumed earlier, this Stokes problem also has $H^2(\Omega) \times H^1(\Omega)$-regularity and the following a priori estimate holds true:

$$\|\mathbf{w}\|_2 + \|\lambda\|_1 \lesssim \|\mathbf{u} - \mathbf{u}_h\|. \tag{41}$$

Let $\mathbf{w}_I \in V_h$ be the *continuous* piecewise linear interpolation of $\mathbf{w}$, then the jump term $[\![\mathbf{w} - \mathbf{w}_I]\!]$ is zero and it is not hard to see that

$$|\!|\!|\mathbf{w} - \mathbf{w}_I|\!|\!| + \|\lambda - \Pi_2 \lambda\| \lesssim h\|\mathbf{u} - \mathbf{u}_h\|. \tag{42}$$

For convenience, denote

$$(\mathbf{v}, \mathbf{w})_{\mathcal{E}_h} = \sum_{e \in \mathcal{E}_h} \int_e \mathbf{v} \cdot \mathbf{w}\, ds.$$

We have the following optimal order L^2 estimate for the velocity.

Theorem 2. *Let $(\mathbf{u}, p) \in (H^2(\Omega) \cap H_0^1(\Omega))^2 \times (L_0^2(\Omega) \cap H^1(\Omega))$ and $(\mathbf{u}_h, p_h) \in V_h \times Q_h$ be the solutions of (1)-(3) and (13)-(14), respectively, with $A(\cdot,\cdot) = A_3(\cdot,\cdot)$. Assuming the body force $\mathbf{f}$ is in $(H^1(\Omega))^2$, then*

$$\|\mathbf{u} - \mathbf{u}_h\| \lesssim h(|\!|\!|\mathbf{u} - \mathbf{u}_h|\!|\!| + \|p - p_h\| + h\|\mathbf{f}\|_1).$$

Proof. Testing (38) by $\mathbf{u} - \mathbf{u}_h$, then using equation (59) and the fact that $\nabla \cdot (\mathbf{u} - \mathbf{u}_h) = 0$ and $(\mathbf{u} - \mathbf{u}_h) \cdot \mathbf{n}$ is continuous across internal edges of $\mathcal{T}_h$, we have

$$\begin{aligned} \|\mathbf{u} - \mathbf{u}_h\|^2 &= -(\mathbf{u} - \mathbf{u}_h,\ \Delta \mathbf{w}) + (\mathbf{u} - \mathbf{u}_h,\ \nabla \lambda) \\ &= (\nabla(\mathbf{u} - \mathbf{u}_h),\ \nabla \mathbf{w})_{\mathcal{T}_h} - \sum_{T \in \mathcal{T}_h} (\nabla \mathbf{w} \cdot \mathbf{n},\ \mathbf{u} - \mathbf{u}_h)_{\partial T} \\ &= (\nabla(\mathbf{u} - \mathbf{u}_h),\ \nabla \mathbf{w})_{\mathcal{T}_h} - (\{\nabla \mathbf{w}\}, [\![\mathbf{u} - \mathbf{u}_h]\!])_{\mathcal{E}_h}. \end{aligned} \tag{43}$$

Meanwhile, subtracting (13)–(14) from (15)–(16), and setting the test function to be $(\mathbf{w}_I, \Pi_2 \lambda)$, yields

$$A(\mathbf{u} - \mathbf{u}_h, \mathbf{w}_I) + C(\mathbf{w}_I, p - p_h) = 0, \tag{44}$$

$$B(\mathbf{u} - \mathbf{u}_h,\ \Pi_2 \lambda) = 0. \tag{45}$$

Using Lemma 1, the definition of γ, and the fact that $\mathbf{w}_I$ is continuous, we have

$$\begin{aligned} &A(\mathbf{u} - \mathbf{u}_h, \mathbf{w}_I) \\ =&(\nabla(\mathbf{u} - \mathbf{u}_h),\ \nabla \mathbf{w}_I)_{\mathcal{T}_h} + (\Delta(\mathbf{u} - \mathbf{u}_h),\ \mathbf{w}_I - \gamma \mathbf{w}_I)_{\mathcal{T}_h} - (\{\nabla \mathbf{w}_I\},\ [\![\mathbf{u} - \mathbf{u}_h]\!])_{\mathcal{E}_h}. \end{aligned}$$

Similarly, using Lemma 2, the facts that $\sum_{T \in \mathcal{T}_h} ((\mathbf{w}_I - \gamma \mathbf{w}_I) \cdot \mathbf{n},\ p - p_h)_{\partial T} = 0$ and $\int_T (\mathbf{w}_I - \gamma \mathbf{w}_I) dx = 0$, we have

$$\begin{aligned} C(\mathbf{w}_I,\ p - p_h) &= -(\nabla \cdot \mathbf{w}_I,\ \ p - p_h)_{\mathcal{T}_h} + \sum_{T \in \mathcal{T}_h} ((\mathbf{w}_I - \gamma \mathbf{w}_I) \cdot \mathbf{n},\ p - p_h)_{\partial T} \\ &\quad - (\nabla(p - p_h),\ \mathbf{w}_I - \gamma \mathbf{w}_I)_{\mathcal{T}_h} \\ &= -(\nabla \cdot \mathbf{w}_I,\ p - p_h)_{\mathcal{T}_h} - (\nabla p,\ \mathbf{w}_I - \gamma \mathbf{w}_I)_{\mathcal{T}_h}. \end{aligned}$$

Substituting the above two equations into (44), subtracting (44) from (43), and using $\nabla \cdot \mathbf{w} = 0$, we have

$$\begin{aligned}
\|\mathbf{u} - \mathbf{u}_h\|^2 &= (\nabla(\mathbf{u} - \mathbf{u}_h),\ \nabla \mathbf{w})_{\mathcal{T}_h} - (\{\nabla \mathbf{w}\},\ [\![\mathbf{u} - \mathbf{u}_h]\!])_{\mathcal{E}_h} \\
&\quad - (\nabla(\mathbf{u} - \mathbf{u}_h),\ \nabla \mathbf{w}_I)_{\mathcal{T}_h} - (\Delta \mathbf{u},\ \mathbf{w}_I - \gamma \mathbf{w}_I)_{\mathcal{T}_h} \\
&\quad + (\{\nabla \mathbf{w}_I\},\ [\![\mathbf{u} - \mathbf{u}_h]\!])_{\mathcal{E}_h} + (\nabla \cdot \mathbf{w}_I,\ p - p_h)_{\mathcal{T}_h} + (\nabla p,\ \mathbf{w}_I - \gamma \mathbf{w}_I)_{\mathcal{T}_h} \\
&= (\nabla(\mathbf{u} - \mathbf{u}_h),\ \nabla(\mathbf{w} - \mathbf{w}_I))_{\mathcal{T}_h} + (-\Delta \mathbf{u} + \nabla p,\ \mathbf{w}_I - \gamma \mathbf{w}_I)_{\mathcal{T}_h} \\
&\quad - (\nabla \cdot (\mathbf{w} - \mathbf{w}_I),\ \ p - p_h)_{\mathcal{T}_h} - (\{\nabla(\mathbf{w} - \mathbf{w}_I)\},\ [\![\mathbf{u} - \mathbf{u}_h]\!])_{\mathcal{E}_h} \\
&\triangleq I_1 + I_2 + I_3 + I_4.
\end{aligned}$$

We estimate I_i, $i = 1, \ldots, 4$, one by one. Using the Schwarz inequality and inequality (42), we have

$$|I_1| = (\nabla(\mathbf{u} - \mathbf{u}_h),\ \nabla(\mathbf{w} - \mathbf{w}_I))_{\mathcal{T}_h} \lesssim |\!|\!|\mathbf{u} - \mathbf{u}_h|\!|\!| |\mathbf{w} - \mathbf{w}_I|_1 \lesssim h \|\mathbf{u} - \mathbf{u}_h\| |\!|\!|\mathbf{u} - \mathbf{u}_h|\!|\!|.$$

An elementary calculation shows that $\int_T (\mathbf{w}_I - \gamma \mathbf{w}_I) dx = 0$ for all $T \in \mathcal{T}_h$. By inequalities (19), (42), we have

$$\begin{aligned}
|I_2| &= (-\Delta \mathbf{u} + \nabla p,\ \mathbf{w}_I - \gamma \mathbf{w}_I)_{\mathcal{T}_h} = (\mathbf{f} - \bar{\mathbf{f}},\ \mathbf{w}_I - \gamma \mathbf{w}_I)_{\mathcal{T}_h} \\
&\lesssim h^2 \|\mathbf{f}\|_1 |\!|\!|\mathbf{w}_I|\!|\!| = h^2 \|\mathbf{f}\|_1 |\mathbf{w}_I|_1 \\
&\lesssim h^2 \|\mathbf{f}\|_1 \|\mathbf{u} - \mathbf{u}_h\|,
\end{aligned}$$

where $\bar{\mathbf{f}}$ is the piecewise constant average of $\mathbf{f}$ over each triangle. It is clear that

$$|I_3| = (\nabla \cdot (\mathbf{w} - \mathbf{w}_I),\ \ p - p_h)_{\mathcal{T}_h} \lesssim h \|\mathbf{u} - \mathbf{u}_h\| \|p - p_h\|$$

Finally, using the Schwartz inequality and inequality (18), we have

$$\begin{aligned}
|I_4| &\lesssim \left(\sum_{e \in \mathcal{E}_h} h_e \|\{\nabla(\mathbf{w} - \mathbf{w}_I)\}\|_e^2 \right)^{\frac{1}{2}} \left(\sum_{e \in \mathcal{E}_h} h_e^{-1} \|[\![\mathbf{u} - \mathbf{u}_h]\!]\|_e^2 \right)^{\frac{1}{2}} \\
&\lesssim h \|\mathbf{u} - \mathbf{u}_h\| |\!|\!|\mathbf{u} - \mathbf{u}_h|\!|\!|.
\end{aligned}$$

Combining all the above gives

$$\|\mathbf{u} - \mathbf{u}_h\| \lesssim h(|\!|\!|\mathbf{u} - \mathbf{u}_h|\!|\!| + \|p - p_h\| + h\|\mathbf{f}\|_1).$$

This completes the proof. □

5.3. An error estimate for the pressure in negative norms. Error estimates in negative norms often reveal important approximation properties that the standard, and commonly used L^2 or H^1 norms are built to ignore. For example, *superconvergence* is one such property that can be identified through an error analysis with negative norms. The goal of this subsection is to establish some error estimate for the pressure approximation in the H^{-1} norm. The result to be presented here suggests a superconvergence for the pressure approximation when correct postprocessing techniques are applied.

Consider the following dual problem: find $(\boldsymbol{\omega}, \xi) \in H_0^1(\Omega)^2 \times L_0^2(\Omega)$ such that

$$-\Delta \boldsymbol{\omega} + \nabla \xi = 0 \qquad \text{in } \Omega, \tag{46}$$

$$\nabla \cdot \boldsymbol{\omega} = \phi \qquad \text{in } \Omega, \tag{47}$$

$$\boldsymbol{\omega} = 0 \qquad \text{on } \partial\Omega, \tag{48}$$

where $\phi \in H^1(\Omega)$ is a given function with the correct compatibility condition. We assume the $H^2(\Omega) \times H^1(\Omega)$-regularity for the solution of the problem (46)-(48):

$$\|\boldsymbol{\omega}\|_2 + \|\xi\|_1 \lesssim \|\phi\|_1. \tag{49}$$

Let $\boldsymbol{\omega}_I \in V_h$ be the *continuous* piecewise linear interpolation of $\boldsymbol{\omega}$, then the jump term $[\![\boldsymbol{\omega} - \boldsymbol{\omega}_I]\!]$ is zero and

$$|||\boldsymbol{\omega} - \boldsymbol{\omega}_I||| + \|\xi - \Pi_2\xi\| \lesssim h\|\phi\|_1. \tag{50}$$

Theorem 3. *Let* $(\mathbf{u}, p) \in (H^2(\Omega) \cap H_0^1(\Omega))^2 \times (L_0^2(\Omega) \cap H^1(\Omega))$ *and* $(\mathbf{u}_h, p_h) \in V_h \times Q_h$ *be the solutions of (1)-(3) and (13)-(14), respectively, with* $A(\cdot,\cdot) = A_3(\cdot,\cdot)$ *and* $\beta = 0$. *Assuming the body force* $\mathbf{f}$ *is in* $(H^1(\Omega))^2$, *then*

$$\|p - p_h\|_{-1} \lesssim h(|||\mathbf{u} - \mathbf{u}_h||| + \|p - p_h\| + h\|\mathbf{f}\|_1).$$

Proof. Subtracting (13)–(14) from (15)–(16), and setting the test function to be $(\boldsymbol{\omega}_I, \Pi_2\xi)$, yields

$$A(\mathbf{u} - \mathbf{u}_h, \boldsymbol{\omega}_I) + C(\boldsymbol{\omega}_I, p - p_h) = 0, \tag{51}$$

$$B(\mathbf{u} - \mathbf{u}_h,\ \Pi_2\xi) = 0. \tag{52}$$

First, testing (47) by $p - p_h$ gives

$$(p - p_h, \phi) = B(\boldsymbol{\omega}, p - p_h) = B(\boldsymbol{\omega} - \boldsymbol{\omega}_I, p - p_h) + B(\boldsymbol{\omega}_I, p - p_h). \tag{53}$$

Using Lemma 2 and the fact that $\sum_{T\in\mathcal{T}_h}((\boldsymbol{\omega}_I - \gamma\boldsymbol{\omega}_I)\cdot\mathbf{n},\ p - p_h)_{\partial T}$ and $\int_T(\boldsymbol{\omega}_I - \gamma\boldsymbol{\omega}_I)dx$ are both zero, we have

$$B(\boldsymbol{\omega}_I, p - p_h) = -C(\boldsymbol{\omega}_I, p - p_h) - (\nabla p,\ \boldsymbol{\omega} - \gamma\boldsymbol{\omega})_{\mathcal{T}_h}. \tag{54}$$

Using (51) and (54), (53) becomes

$$(p - p_h, \phi) = B(\boldsymbol{\omega} - \boldsymbol{\omega}_I, p - p_h) + A(\mathbf{u} - \mathbf{u}_h, \boldsymbol{\omega}_I) - (\nabla p,\ \boldsymbol{\omega} - \gamma\boldsymbol{\omega})_{\mathcal{T}_h}. \tag{55}$$

Testing (46) by $\mathbf{u} - \mathbf{u}_h$, then using equation (59) and the fact that $\nabla\cdot(\mathbf{u} - \mathbf{u}_h) = 0$ and $(\mathbf{u} - \mathbf{u}_h)\cdot\mathbf{n}$ is continuous across internal edges of $\mathcal{T}_h$, we have

$$\begin{aligned} 0 &= -(\mathbf{u} - \mathbf{u}_h,\ \Delta\boldsymbol{\omega}) + (\mathbf{u} - \mathbf{u}_h,\ \nabla\xi) \\ &= (\nabla(\mathbf{u} - \mathbf{u}_h),\ \nabla\boldsymbol{\omega})_{\mathcal{T}_h} - \sum_{T\in\mathcal{T}_h}(\nabla\boldsymbol{\omega}\cdot\mathbf{n},\ \mathbf{u} - \mathbf{u}_h)_{\partial T} \\ &= (\nabla(\mathbf{u} - \mathbf{u}_h),\ \nabla\boldsymbol{\omega})_{\mathcal{T}_h} - (\{\nabla\boldsymbol{\omega}\}, [\![\mathbf{u} - \mathbf{u}_h]\!])_{\mathcal{E}_h}. \end{aligned} \tag{56}$$

Using Lemma 1, the definition of γ, and the fact that $\boldsymbol{\omega}_I$ is continuous, we have

$$\begin{aligned} &A(\mathbf{u} - \mathbf{u}_h, \boldsymbol{\omega}_I) \\ =&(\nabla(\mathbf{u} - \mathbf{u}_h),\ \nabla\boldsymbol{\omega}_I)_{\mathcal{T}_h} + (\Delta(\mathbf{u} - \mathbf{u}_h),\ \boldsymbol{\omega}_I - \gamma\boldsymbol{\omega}_I)_{\mathcal{T}_h} - (\{\nabla\boldsymbol{\omega}_I\},\ [\![\mathbf{u} - \mathbf{u}_h]\!])_{\mathcal{E}_h}. \end{aligned}$$

Substituting the above equation into (55), then subtracting (56) from (55), we have

$$\begin{aligned} (p - p_h, \phi) &= B(\boldsymbol{\omega} - \boldsymbol{\omega}_I, p - p_h) + (\nabla(\mathbf{u} - \mathbf{u}_h),\ \nabla\boldsymbol{\omega}_I)_{\mathcal{T}_h} + (\Delta\mathbf{u},\ \boldsymbol{\omega}_I - \gamma\boldsymbol{\omega}_I)_{\mathcal{T}_h} \\ &- (\{\nabla\boldsymbol{\omega}_I\},\ [\![\mathbf{u} - \mathbf{u}_h]\!])_{\mathcal{E}_h} - (\nabla(\mathbf{u} - \mathbf{u}_h),\ \nabla\boldsymbol{\omega})_{\mathcal{T}_h} + (\{\nabla\boldsymbol{\omega}\},\ [\![\mathbf{u} - \mathbf{u}_h]\!])_{\mathcal{E}_h} \\ &- (\nabla p,\ \boldsymbol{\omega} - \gamma\boldsymbol{\omega})_{\mathcal{T}_h} \\ &= B(\boldsymbol{\omega} - \boldsymbol{\omega}_I, p - p_h) - (\nabla(\mathbf{u} - \mathbf{u}_h),\ \nabla(\boldsymbol{\omega} - \boldsymbol{\omega}_I))_{\mathcal{T}_h} \\ &+ (\Delta\mathbf{u} - \nabla p,\ \boldsymbol{\omega}_I - \gamma\boldsymbol{\omega}_I)_{\mathcal{T}_h} + (\{\nabla(\boldsymbol{\omega} - \boldsymbol{\omega}_I)\},\ [\![\mathbf{u} - \mathbf{u}_h]\!])_{\mathcal{E}_h} \\ &= I_1 + I_2 + I_3 + I_4. \end{aligned}$$

Using the Schwarz inequality and inequality (50), we have

$$|I_1| = B(\boldsymbol{\omega} - \boldsymbol{\omega}_I, p - p_h) \lesssim \|p - p_h\||\boldsymbol{\omega} - \boldsymbol{\omega}_I|_1 \lesssim h\|\phi\|_1\|p - p_h\|.$$

and

$$|I_2| = (\nabla(\mathbf{u} - \mathbf{u}_h),\ \nabla(\boldsymbol{\omega} - \boldsymbol{\omega}_I))_{\mathcal{T}_h} \lesssim |||\mathbf{u} - \mathbf{u}_h|||\boldsymbol{\omega} - \boldsymbol{\omega}_I|_1 \lesssim h\|\phi\|_1|||\mathbf{u} - \mathbf{u}_h|||.$$

Using the fact $\int_T(\boldsymbol{\omega}_I - \gamma\boldsymbol{\omega}_I)dx = 0$ for all $T \in \mathcal{T}_h$ and the inequalities (19), (50), we have

$$\begin{aligned} |I_3| &= (\Delta\mathbf{u} - \nabla p,\ \boldsymbol{\omega}_I - \gamma\boldsymbol{\omega}_I)_{\mathcal{T}_h} = (\mathbf{f} - \bar{\mathbf{f}},\ \gamma\boldsymbol{\omega}_I - \boldsymbol{\omega}_I)_{\mathcal{T}_h} \\ &\lesssim h^2\|\mathbf{f}\|_1|||\boldsymbol{\omega}_I||| = h^2\|\mathbf{f}\|_1|\boldsymbol{\omega}_I|_1 \\ &\lesssim h^2\|\mathbf{f}\|_1\|\phi\|_1, \end{aligned}$$

where $\bar{\mathbf{f}}$ is the piecewise constant average of $\mathbf{f}$ over each triangle.

Using the Schwartz inequality and inequality (18), we have

$$\begin{aligned} |I_4| &\lesssim \left(\sum_{e\in\mathcal{E}_h} h_e\|\{\nabla(\boldsymbol{\omega} - \boldsymbol{\omega}_I)\}\|_e^2\right)^{\frac{1}{2}} \left(\sum_{e\in\mathcal{E}_h} h_e^{-1}\|[\![\mathbf{u} - \mathbf{u}_h]\!]\|_e^2\right)^{\frac{1}{2}} \\ &\lesssim h\|\phi\|_1|||\mathbf{u} - \mathbf{u}_h|||. \end{aligned}$$

Combining all the above gives

$$\|p - p_h\|_{-1} \lesssim h(|||\mathbf{u} - \mathbf{u}_h||| + \|p - p_h\| + h\|\mathbf{f}\|_1).$$

This completes the proof. □

6. A divergence-free finite volume formulation

Observe that the velocity field in discrete equations (13)–(14) is exactly divergence-free. Thus, it is natural to solve for the velocity from a divergence free subspace D_h:

$$D_h = \{\mathbf{v} \in V_h;\ \nabla \cdot \mathbf{v} = 0\}.$$

In particular, by restricting the test function to the subspace D_h, the discrete formulation (13)-(14) can be reduced into the following divergence-free finite volume scheme: find $\mathbf{u}_h \in D_h$ such that

$$A(\mathbf{u}_h, \mathbf{v}) = (\mathbf{f}, \gamma\mathbf{v}) \qquad \text{for all } \mathbf{v} \in D_h. \tag{57}$$

The above formulation has several advantages in practical computation. First, it eliminates the pressure from a coupled system and therefore avoids the solution of a saddle point problem of very large scale. Secondly, the problem (57) is symmetric and positive definite if the form $A(\mathbf{v}, \mathbf{w}) = A_3(\mathbf{v}, \mathbf{w})$ was used. Consequently, the resulting matrix problem can be solved by some existing conjugate gradient methods. In addition, there are methods available for developing efficient preconditioners for symmetric and positive definite problems. The formulation (57) is particularly attractive in cases where the velocity is the primary variable of interest, such as the application of groundwater flow simulation.

In the computational implementation for (57), one needs to know the structure of the subspace D_h. In fact, a computable basis for the divergence-free subspace D_h can be derived by using the potential from the Helmholtz decomposition. For problems with two spacial variables, a divergence-free vector $\mathbf{v}$ admits a potential function ϕ and

$$\mathbf{v} = \text{curl}\phi := \begin{pmatrix} -\partial_y\phi \\ \partial_x\phi \end{pmatrix}.$$

For the Brezzi-Douglas-Marini (BDM) elements, the following result is well-known [4, 17, 18]:

Theorem 4. *There exists a one-to-one map* curl : $S_h \to D_h$, *where the stream-function space* S_h *is defined as following:*

$$S_h = \{\phi \in H_0^1(\Omega);\ \phi|_T \in P_2(T),\ T \in \mathcal{T}_h\}. \tag{58}$$

According to this theorem, one can derive a computable basis for D_h by simply taking curl of the nodal basis of P_2 conforming elements.

7. Numerical examples

In this section, we present some numerical results for the new discretization scheme. All the numerical experiments are conducted on the Stokes equation defined on the unit square domain $\Omega = (0,1) \times (0,1)$ with uniform triangulations. The triangulations are constructed as follows: (1) partition the domain into an $n \times n$ rectangular mesh, and (2) divide each square element into two triangles by the diagonal line with a negative slope. We use $\mathcal{T}_h$ to denote the uniform triangular mesh with mesh size $h = 1/n$. Here we only report results for $\beta = 0$. The results for $\beta > 0$ are similar.

The test problem 1 assumes the Stokes problem has an exact solution of $\mathbf{u} = (u_1, u_2)$ and p where

$$u_1 = -2x^2(x-1)^2y(y-1)(2y-1), \quad u_2 = 2y^2(y-1)^2x(x-1)(2x-1)$$

and

$$p = x^2 + y^2 - 2/3.$$

It can be seen that the exact solution satisfies the following conditions:

$$\mathbf{u}|_{\partial\Omega} = \mathbf{0}, \qquad \int_\Omega p\, dx = 0.$$

The tested numerical scheme uses the form $A(\cdot,\cdot) = A_3(\cdot,\cdot)$ with a parameter value of $\alpha = 10$. The resulting linear system, which is symmetric but indefinite, was solved by using the MINRES (minimum residual) method. The iteration was stopped when the relative residual reaches $1e-12$. The error on different meshes are reported in Table 1, in which

$$\|\mathbf{u} - \mathbf{u}_h\|_{\mathcal{E}_h} = \left(\sum_{e \in \mathcal{E}_h} h_e^{-1} \|\mathbf{u} - \mathbf{u}_h\|_e^2 \right)^{1/2}.$$

The numerical result indicates a convergence of order $O(h^2)$ for the velocity in the standard L^2 norm, $O(h)$ for the velocity in an equivalent H^1 norm, and $O(h)$ for the pressure in the standard L^2 norm. The numerical results are in accordance with the theoretical prediction as established in previous sections.

It was observed that the numerical approximation for the pressure unknown sometimes possesses a certain oscillation around the exact solution (see Figure 2 for the pressure plot and the left one in Figure 3). To obtain a pressure approximation with better accuracy, we investigated a simple postprocessing method for the pressure approximation by using a local averaging method. More precisely, the postprocessing method allows us to construct a new pressure approximation at each interior nodal point by taking the average of the pressure approximations at six triangles that share the node as a vertex point. This post-processed pressure approximation is denoted by $\tilde{p}_h$ and an error in a discrete maximum norm (at all interior nodal points) was computed and reported in the table. This error is denoted as $\|p - \tilde{p}_h\|_{max}$ in all the tables. It is clear that the post-processed pressure has smaller errors with a much faster convergence. The numerical plot (see the right plot in Figure 3) shows a much improved pressure approximation.

The numerical algorithm presented in this paper can be extended to problems with nonhomogeneous Dirichlet boundary conditions without any difficulty. For

TABLE 1. Numerical results for test problem 1: $\mathbf{u}\cdot\mathbf{n}=0, \mathbf{u}\cdot\mathbf{t}=0, \alpha=10$, with form A_3 and exact solution $u_1=-2x^2y(x-1)^2(2y-1)(y-1)$, $u_2=2xy^2(2x-1)(x-1)(y-1)^2$, $p=x^2+y^2-2/3$

mesh size h	$\|\mathbf{u}-\mathbf{u}_h\|$	$\|\mathbf{u}-\mathbf{u}_h\|_1$	$\|\mathbf{u}-\mathbf{u}_h\|_{\mathcal{E}_h}$	$\|p-p_h\|$	$\|p-\tilde{p}_h\|_{max}$
1/16	3.53e-04	1.57e-02	3.01e-03	4.10e-02	6.60e-03
1/20	2.33e-04	1.25e-02	2.45e-03	3.29e-02	4.58e-03
1/24	1.64e-04	1.04e-02	2.06e-03	2.75e-02	3.41e-03
1/28	1.22e-04	8.94e-03	1.78e-03	2.36e-02	2.64e-03
1/32	9.38e-05	7.82e-03	1.56e-03	2.07e-02	2.14e-03
1/36	7.50e-05	6.94e-03	1.39e-03	1.84e-02	1.82e-03
1/40	6.09e-05	6.25e-03	1.25e-03	1.66e-02	1.66e-03
1/44	5.05e-05	5.68e-03	1.14e-03	1.51e-02	1.42e-03
1/48	4.25e-05	5.20e-03	1.05e-03	1.38e-02	1.01e-03
1/52	3.62e-05	4.80e-03	9.69e-04	1.28e-02	8.77e-04
1/56	3.12e-05	4.46e-03	9.00e-04	1.19e-02	7.70e-04
1/60	2.72e-05	4.16e-03	8.41e-04	1.11e-02	6.81e-04
1/64	2.39e-05	3.90e-03	7.88e-04	1.04e-02	6.08e-04
Asym. Rate	1.9479	1.0047	0.9711	0.9892	1.7153

example, the standard Dirichlet boundary condition of

$$\mathbf{u}=\mathbf{g} \qquad \text{on } \partial\Omega.$$

can be implemented by imposing both $\mathbf{u}\cdot\mathbf{n}=\mathbf{g}\cdot\mathbf{n}$ and $\mathbf{u}\cdot\mathbf{t}=\mathbf{g}\cdot\mathbf{t}$ as boundary conditions, where $\mathbf{n}$ is the normal direction and $\mathbf{t}$ is the tangential direction of $\partial\Omega$. It should be pointed out that such an implementation should treat $\mathbf{u}\cdot\mathbf{n}=\mathbf{g}\cdot\mathbf{n}$ as an essential boundary condition and $\mathbf{u}\cdot\mathbf{t}=\mathbf{g}\cdot\mathbf{t}$ as a natural boundary condition. The part of the natural boundary condition corresponds to a modification of the original right-hand side, which is $(\mathbf{f},\gamma\mathbf{v}_h)$, as follows:

$$\begin{cases} A_1(\cdot,\cdot): & (\mathbf{f},\gamma\mathbf{v}_h)+\alpha\sum_e\int_e h_e^{-1}(\mathbf{g}\cdot\mathbf{t})[\![\mathbf{v}_h]\!]ds, \\ A_2(\cdot,\cdot): & (\mathbf{f},\gamma\mathbf{v}_h)+\alpha\sum_e\int_e h_e^{-1}(\mathbf{g}\cdot\mathbf{t})[\![\mathbf{v}_h]\!]ds+\sum_e\int_e\{\nabla\mathbf{v}_h\}(\mathbf{g}\cdot\mathbf{t})ds, \\ A_3(\cdot,\cdot): & (\mathbf{f},\gamma\mathbf{v}_h)+\alpha\sum_e\int_e h_e^{-1}(\mathbf{g}\cdot\mathbf{t})[\![\mathbf{v}_h]\!]ds-\sum_e\int_e\{\nabla\mathbf{v}_h\}(\mathbf{g}\cdot\mathbf{t})ds. \end{cases}$$

The numerical scheme was tested on several other examples. The second test problem assumes the following exact solution for the Stokes problem:

$$\mathbf{u}=\begin{pmatrix}\sin(2\pi x)\cos(2\pi y)\\ -\cos(2\pi x)\sin(2\pi y)\end{pmatrix},\ p=x^2+y^2-2/3.$$

It is not hard to see that for test problem 2, the boundary condition is homogeneous for $\mathbf{u}\cdot\mathbf{n}$, but non-homogeneous for $\mathbf{u}\cdot\mathbf{t}$. The third test problem assumes the following exact solution

$$\mathbf{u}=\begin{pmatrix}\cos(2\pi x)\sin(2\pi y)\\ -\sin(2\pi x)\cos(2\pi y)\end{pmatrix},\ p=0,$$

for which one has $\mathbf{u}\cdot\mathbf{n}\neq 0$ and $\mathbf{u}\cdot\mathbf{t}=0$ on $\partial\Omega$. Again, the test problems 2 and 3 were approximated by using the form $A_3(\cdot,\cdot)$ with $\alpha=10$ and the linear solver assumed a stopping criterion with relative residual $1e-12$. The results are reported in Tables 2 and 3.

TABLE 2. Numerical results for test problem 2: $\mathbf{u}\cdot\mathbf{n}=0, \mathbf{u}\cdot\mathbf{t}\neq 0, \alpha=10$, with form A_3 and exact solution of $u_1=\sin(2\pi x)\cos(2\pi y)$, $u_2=-\cos(2\pi x)\sin(2\pi y)$, $p=x^2+y^2-2/3$

mesh size h	$\|\mathbf{u}-\mathbf{u}_h\|$	$\|\mathbf{u}-\mathbf{u}_h\|_1$	$\|\mathbf{u}-\mathbf{u}_h\|_{\mathcal{E}_h}$	$\|p-p_h\|$	$\|p-\tilde{p}_h\|_{max}$
1/16	5.67e-02	1.79e+00	4.60e-01	2.46e+00	9.63e-01
1/20	3.77e-02	1.43e+00	3.79e-01	2.04e+00	6.96e-01
1/24	2.67e-02	1.19e+00	3.21e-01	1.73e+00	5.17e-01
1/28	1.99e-02	1.02e+00	2.78e-01	1.51e+00	4.02e-01
1/32	1.53e-02	8.94e-01	2.45e-01	1.33e+00	3.19e-01
1/36	1.22e-02	7.94e-01	2.19e-01	1.19e+00	2.61e-01
1/40	9.96e-03	7.14e-01	1.98e-01	1.07e+00	2.16e-01
1/44	8.26e-03	6.49e-01	1.80e-01	9.84e-01	1.83e-01
1/48	6.96e-03	5.94e-01	1.66e-01	9.04e-01	1.56e-01
1/52	5.94e-03	5.49e-01	1.53e-01	8.36e-01	1.36e-01
1/56	5.13e-03	5.09e-01	1.42e-01	7.78e-01	1.18e-01
1/60	4.47e-03	4.75e-01	1.33e-01	7.27e-01	1.04e-01
1/64	3.93e-03	4.45e-01	1.25e-01	6.83e-01	9.33e-02
Asym. Order	1.9330	1.0056	0.9470	0.9343	1.7034

In all three test cases, we examined the error for the post-processed pressure $\tilde{p}_h$ whose value at each interior node is calculated by taking average of neighboring triangles. The numerical results demonstrate a convergence of order between $O(h^{1.5})$ and $O(h^2)$ for the post-processed pressure approximation. The pressure approximation p_h was theoretically and numerically known to be of order $O(h)$ accurate. Therefore, the post-processed pressure approximation $\tilde{p}_h$ is very likely of superconvergent. The error analysis for the pressure shows an accuracy of $O(h^2)$ in the H^{-1} norm, which is believed to indicate a superconvergence for the pressure approximation with order of $O(h^2)$ at some spacial locations yet to be determined. Interested readers are encouraged to investigate this superconvergence from a theoretical point of view. We emphasize that this possible superconvergence should be dependent of the mesh uniformity.

We also explored the effect of different values of α on the errors for a test problem with exact solution given by

$$\mathbf{u}=\begin{pmatrix}-x(x-1)(2y-1)\\ y(2x-1)(y-1)\end{pmatrix}, \quad q=x^2+y^2-2/3.$$

Observe that this test problem has non-homogeneous boundary conditions for both the essential and the natural data. Again, the numerical test results were computed by using the form $A_3(\cdot,\cdot)$ with mesh size $h=1/16$. The MINRES iteration stops at a relative residual of $1e-12$. The errors at various norms for both the velocity and the pressure approximation are reported in Table 4. Since $A_3(\cdot,\cdot)$ is only coercive for α large enough, the extremely large iteration number (which is not reported in this table) for the case of $\alpha=1$ might indicate that $A_3(\cdot,\cdot)$ is not coercive. It can be seen that the error in L^2 and H^1 norm for the velocity approximation is not effected much by varying α. However, the error quantity $\|\mathbf{u}-\mathbf{u}_h\|_{\mathcal{E}_h}$, which measures the jump of the velocity along edges, is supposed to get smaller as α increases. This theoretical prediction is clearly demonstrated by the numerical experiments as shown in Table 4. It is also interesting to note that the pressure

TABLE 3. Numerical results for test problem 3: $\mathbf{u}\cdot\mathbf{n}\neq 0, \mathbf{u}\cdot\mathbf{t}=0, \alpha=10$, with form A_3 and exact solution of $u_1=\cos(2\pi x)\sin(2\pi y)$, $u_2=-\sin(2\pi x)\cos(2\pi y)$, $p=0$

mesh size h	$\|\mathbf{u}-\mathbf{u}_h\|$	$\|\mathbf{u}-\mathbf{u}_h\|_1$	$\|\mathbf{u}-\mathbf{u}_h\|_{\mathcal{E}_h}$	$\|p-p_h\|$	$\|p-\tilde{p}_h\|_{max}$
1/16	6.69e-02	1.79e+00	4.57e-01	2.47e+00	9.24e-01
1/20	4.41e-02	1.43e+00	3.77e-01	2.04e+00	6.77e-01
1/24	3.12e-02	1.19e+00	3.20e-01	1.74e+00	5.09e-01
1/28	2.32e-02	1.02e+00	2.78e-01	1.51e+00	3.97e-01
1/32	1.78e-02	8.94e-01	2.45e-01	1.33e+00	3.18e-01
1/36	1.42e-02	7.94e-01	2.19e-01	1.19e+00	2.60e-01
1/40	1.15e-02	7.14e-01	1.97e-01	1.07e+00	2.17e-01
1/44	9.57e-03	6.49e-01	1.80e-01	9.84e-01	1.84e-01
1/48	8.06e-03	5.95e-01	1.65e-01	9.04e-01	1.57e-01
1/52	6.87e-03	5.49e-01	1.53e-01	8.37e-01	1.36e-01
1/56	5.93e-03	5.09e-01	1.42e-01	7.78e-01	1.20e-01
1/60	5.17e-03	4.75e-01	1.33e-01	7.27e-01	1.06e-01
1/64	4.55e-03	4.45e-01	1.24e-01	6.83e-01	9.44e-02
Asym. Order	1.9461	1.0067	0.9434	0.9348	1.6679

TABLE 4. Numerical results for test problem 4: $\mathbf{u}\cdot\mathbf{n}\neq 0, \mathbf{u}\cdot\mathbf{t}\neq 0$, mesh size $16x16$, with form A_3 and exact solution of $u_1=-x(x-1)(2y-1)$, $u_2=y(2x-1)(y-1)$, $p=x^2+y^2-2/3$.

α	$\|\mathbf{u}-\mathbf{u}_h\|$	$\|\mathbf{u}-\mathbf{u}_h\|_1$	$\|\mathbf{u}-\mathbf{u}_h\|_{\mathcal{E}_h}$	$\|p-p_h\|$	$\|p-\tilde{p}_h\|_{max}$
1	1.354931e-02	5.034632e-01	4.586401e-01	8.594745e-02	2.144773e-01
2	3.026899e-03	1.480872e-01	8.044606e-02	4.250402e-02	1.731431e-02
3	1.421309e-03	9.584819e-02	3.667362e-02	4.963551e-02	6.597814e-03
4	1.250238e-03	9.116745e-02	3.048267e-02	6.186949e-02	7.295428e-03
5	1.240441e-03	9.087715e-02	2.979724e-02	7.563794e-02	7.926560e-03
6	1.239846e-03	9.082193e-02	2.956330e-02	9.030884e-02	8.534093e-03
7	1.240552e-03	9.081191e-02	2.944909e-02	1.054993e-01	9.109844e-03
8	1.241371e-03	9.081424e-02	2.938203e-02	1.210116e-01	9.653780e-03
9	1.242123e-03	9.082025e-02	2.933951e-02	1.367445e-01	1.017644e-02
10	1.242826e-03	9.082717e-02	2.931257e-02	1.526427e-01	1.068873e-02
20	1.244702e-03	9.087593e-02	2.924709e-02	3.150176e-01	1.582171e-02
30	1.243157e-03	9.089947e-02	2.923661e-02	4.790511e-01	2.141916e-02
40	1.241231e-03	9.091501e-02	2.923345e-02	6.434840e-01	2.677698e-02

approximation is somewhat sensitive to the values of α. For example, $\|p-p_h\|$ seems to first decrease and then increase as the value of α increases. The numerical results shown in Table 4 suggest that the best result allowed for a given mesh may have already been reached at $\alpha=4$. Table 5 shows the performance of the numerical scheme with $\alpha=3.5$. The results in Table 5 should be compared with those in Table 3.

TABLE 5. Numerical results for test problem 3: $\mathbf{u}\cdot\mathbf{n}\neq 0, \mathbf{u}\cdot\mathbf{t}=0, \alpha=3.5$, with form A_3 and exact solution of $u_1=\cos(2\pi x)\sin(2\pi y)$, $u_2=-\sin(2\pi x)\cos(2\pi y)$, $p=0$

mesh size h	$\|\mathbf{u}-\mathbf{u}_h\|$	$\|\mathbf{u}-\mathbf{u}_h\|_1$	$\|\mathbf{u}-\mathbf{u}_h\|_{\mathcal{E}_h}$	$\|p-p_h\|$	$\|p-\tilde{p}_h\|_{max}$
1/16	4.32e-02	1.81e+00	5.78e-01	8.19e-01	5.06e-01
1/20	2.82e-02	1.45e+00	4.57e-01	6.68e-01	3.79e-01
1/24	1.98e-02	1.20e+00	3.75e-01	5.63e-01	2.88e-01
1/28	1.47e-02	1.03e+00	3.16e-01	4.86e-01	2.25e-01
1/32	1.13e-02	9.01e-01	2.73e-01	4.27e-01	1.81e-01
1/36	8.97e-03	8.00e-01	2.40e-01	3.81e-01	1.48e-01
1/40	7.28e-03	7.19e-01	2.14e-01	3.44e-01	1.23e-01
1/44	6.03e-03	6.53e-01	1.94e-01	3.13e-01	1.04e-01
1/48	5.07e-03	5.98e-01	1.76e-01	2.87e-01	8.98e-02
1/52	4.32e-03	5.51e-01	1.62e-01	2.65e-01	7.79e-02
1/56	3.73e-03	5.11e-01	1.50e-01	2.47e-01	6.81e-02
1/60	3.25e-03	4.77e-01	1.39e-01	2.30e-01	6.01e-02
1/64	2.86e-03	4.47e-01	1.30e-01	2.16e-01	5.35e-02
Asym. Order	1.9633	1.0116	1.0780	0.9643	1.6506

FIGURE 2. Numerical solution for u_1 (top-left), u_2 (top-right), and p (bottom-left) for test problem 3: $\alpha=3.5$, mesh=16×16 with form A_3 and exact solution of $u_1=\cos(2\pi x)\sin(2\pi y)$, $u_2=-\sin(2\pi x)\cos(2\pi y)$, $p=0$.

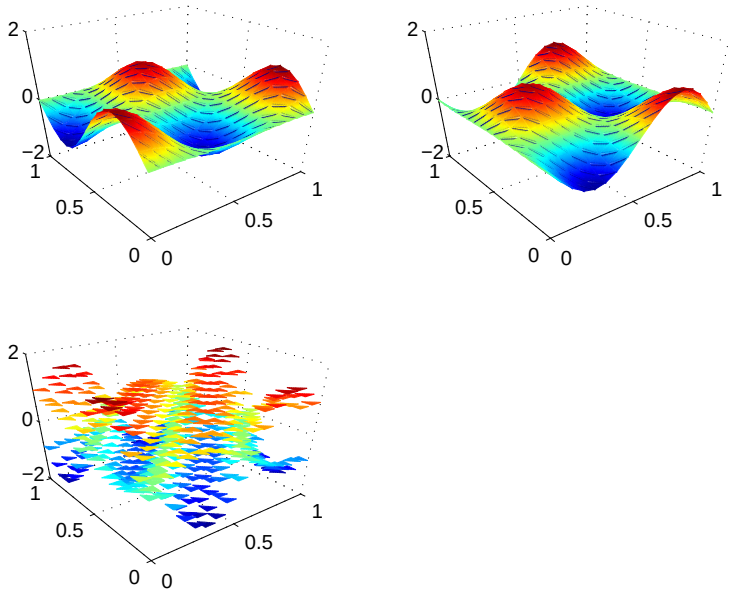

Appendix A. Proof of Lemma 1 and 2

A straightforward computation gives

$$\sum_{T\in\mathcal{T}_h}\int_{\partial T}\mathbf{v}\cdot(\tau\mathbf{n})ds = \sum_{e\in\mathcal{E}_h^0}\int_e[\tau]\cdot\{\mathbf{v}\}ds+\sum_{e\in\mathcal{E}_h}\int_e\{\tau\}:[\![\mathbf{v}]\!]ds. \tag{59}$$

FIGURE 3. Numerical solution for the pressure (left) and its post-processed version $\tilde{p}_h$ (right) for test problem 3: $\alpha = 3.5$, mesh=64$\times$64 with form A_3 and exact solution of $u_1 = \cos(2\pi x)\sin(2\pi y)$, $u_2 = -\sin(2\pi x)\cos(2\pi y)$, $p = 0$.

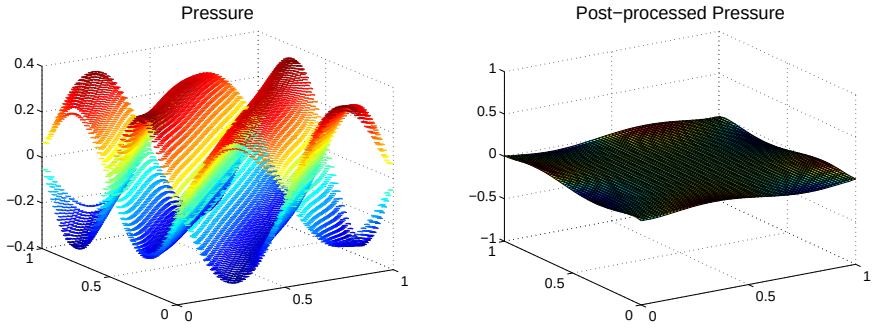

We first prove lemma 1.

Proof. From Figure 1, it is not hard to see that for $\mathbf{v}$, $\mathbf{w} \in V(h)$,

$$A_0(\mathbf{v},\mathbf{w}) = -\sum_{T\in\mathcal{T}_h}\sum_{j=1}^{3}\int_{A_{j+1}CA_j}\frac{\partial \mathbf{v}}{\partial \mathbf{n}}\cdot\gamma\mathbf{w}ds - \sum_{e\subset\partial\Omega}\int_e\frac{\partial \mathbf{v}}{\partial \mathbf{n}}\cdot\gamma\mathbf{w}ds. \tag{60}$$

Here we denote vertex $A_4 = A_1$ for convenience. The integral on $A_{j+1}CA_j$ should be understood as integration along the joint of line segments $A_{j+1}C$ and CA_j, and the outward normal $\mathbf{n}$ is set with respect to each subtriangle S_i, $i = 1, 2, 3$.

Using the divergence theorem on each subtriangle S_j shown in Figure 1, and notice that $\gamma\mathbf{w}$ is a constant on each S_j, we have

$$\begin{aligned}
&-\sum_{T\in\mathcal{T}_h}\sum_{j=1}^{3}\int_{A_{j+1}CA_j}\frac{\partial \mathbf{v}}{\partial \mathbf{n}}\cdot\gamma\mathbf{w}ds\\
=&\sum_{T\in\mathcal{T}_h}\sum_{j=1}^{3}\int_{A_jA_{j+1}}\frac{\partial \mathbf{v}}{\partial \mathbf{n}}\cdot\gamma\mathbf{w}ds - \sum_{T\in\mathcal{T}_h}\sum_{S_j\subset T}(\Delta\mathbf{v},\gamma\mathbf{w})_{S_j}\\
=&\sum_{T\in\mathcal{T}_h}\int_{\partial T}(\gamma\mathbf{w}-\mathbf{w})\cdot\frac{\partial \mathbf{v}}{\partial \mathbf{n}}ds + \sum_{T\in\mathcal{T}_h}\int_{\partial T}\mathbf{w}\cdot\frac{\partial \mathbf{v}}{\partial \mathbf{n}}ds - (\Delta\mathbf{v},\,\gamma\mathbf{w})_{\mathcal{T}_h}\\
=&(\nabla\mathbf{v},\nabla\mathbf{w})_{\mathcal{T}_h} + \sum_{T\in\mathcal{T}_h}\int_{\partial T}(\gamma\mathbf{w}-\mathbf{w})\cdot\frac{\partial \mathbf{v}}{\partial \mathbf{n}}ds + (\Delta\mathbf{v},\mathbf{w}-\gamma\mathbf{w})_{\mathcal{T}_h}.
\end{aligned} \tag{61}$$

Using (59) and the definition of γ, the second term becomes

$$\begin{aligned}
&\sum_{T\in\mathcal{T}_h}\int_{\partial T}(\gamma\mathbf{w}-\mathbf{w})\cdot\frac{\partial \mathbf{v}}{\partial \mathbf{n}}ds\\
=&\sum_{e\subset\partial\Omega}\int_e\frac{\partial \mathbf{v}}{\partial \mathbf{n}}\cdot\gamma\mathbf{w}ds - \sum_{e\in\mathcal{E}_h}\int_e\{\nabla\mathbf{v}\}:[\![\mathbf{w}]\!]ds \quad + \sum_{e\in\mathcal{E}_h^0}\int_e[\nabla\mathbf{v}]\cdot\{\gamma\mathbf{w}-\mathbf{w}\}ds.
\end{aligned}$$

Combining (60), (61) and the above gives Equation (9). For $\mathbf{v} \in V_h$, both $\sum_{e\in\mathcal{E}_h^0}\int_e[\nabla\mathbf{v}]\cdot\{\gamma\mathbf{w}-\mathbf{w}\}ds$ and $(\Delta\mathbf{v}, \mathbf{w}-\gamma\mathbf{w})_{\mathcal{T}_h}$ vanishes, by the properties of V_h and γ. This completes the proof of Lemma 1. □

Next we prove Lemma 2.

Proof. Notice that all $\mathbf{v} \in V(h)$ satisfy the boundary condition $\mathbf{v}\cdot\mathbf{n} = 0$ on $\partial\Omega$. By the definition of γ, we have $\gamma\mathbf{v}\cdot\mathbf{n} = 0$ on $\partial\Omega$. Hence, using the divergence theorem on each subtriangle S_j for $\mathbf{v} \in V(h)$,

$$
\begin{aligned}
C(\mathbf{v}, q) &= \sum_{T\in\mathcal{T}_h}\sum_{j=1}^{3}\int_{A_{j+1}CA_j}\gamma\mathbf{v}\cdot\mathbf{n}qds \\
&= -\sum_{T\in\mathcal{T}_h}\sum_{j=1}^{3}\int_{A_jA_{j+1}}\gamma\mathbf{v}\cdot\mathbf{n}qds + \sum_{T\in\mathcal{T}_h}\sum_{S_j\subset T}(\nabla q,\ \gamma\mathbf{v})_{T_j} \\
&= \sum_{T\in\mathcal{T}_h}\int_{\partial T}(\mathbf{v}-\gamma\mathbf{v})\cdot\mathbf{n}qds - \sum_{T\in\mathcal{T}_h}\int_{\partial T}\mathbf{v}\cdot\mathbf{n}qds + (\nabla q, \gamma\mathbf{v})_{\mathcal{T}_h} \\
&= \sum_{T\in\mathcal{T}_h}\int_{\partial T}(\mathbf{v}-\gamma\mathbf{v})\cdot\mathbf{n}qds + (\nabla q, \gamma\mathbf{v})_{\mathcal{T}_h} - (\nabla q, \mathbf{v})_{\mathcal{T}_h} - (\nabla\cdot\mathbf{v}, q)_{\mathcal{T}_h} \\
&= -(\nabla\cdot\mathbf{v},\ q)_{\mathcal{T}_h} + \sum_{T\in\mathcal{T}_h}\int_{\partial T}(\mathbf{v}-\gamma\mathbf{v})\cdot\mathbf{n}qds + (\nabla q, \gamma\mathbf{v}-\mathbf{v})_{\mathcal{T}_h}.
\end{aligned}
$$

If $q \in Q_h$, the third term in the above expression obviously vanishes. The second term also vanishes since $(\mathbf{v}-\gamma\mathbf{v})\cdot\mathbf{n}$ is continuous across the edges of $\mathcal{T}_h$ and hence by definition we have

$$
\int_e(\mathbf{v}-\gamma\mathbf{v})\cdot\mathbf{n}\,ds = 0 \qquad \text{for all } e \in \mathcal{E}_h.
$$

This completes the proof of Lemma 2. □

Appendix B. Proof of inequalities (19) and (20)

We first prove inequality (19). Since each $T \in \mathcal{T}_h$ is composed of three subtriangles, we have

$$
\|\mathbf{v}-\gamma\mathbf{v}\|_{\mathcal{T}_h}^2 = \sum_{T\in\mathcal{T}_h}\sum_{j=1}^{3}\|\mathbf{v}-\gamma\mathbf{v}\|_{S_j}^2.
$$

The proof will be done on each subtriangle.

Let S be a subtriangle and e, with length h_e, be the edge of S that belongs to $\mathcal{E}_h$. By the Bramble-Hilbert lemma, it is easy to see that for all $\mathbf{v} \in (H^2(S))^2$, we have

$$
\|\mathbf{v} - \frac{1}{h_e}\int_e\mathbf{v}\,ds\|_S \lesssim h|\mathbf{v}|_{1,S}. \tag{62}
$$

Therefore, on each subtriangle whose chosen edge e is on $\partial\Omega$, the statement in inequality (19) is automatically true. We only need to consider subtriangles associated with internal edges.

Let $T_1, T_2 \in \mathcal{T}_h$ be two triangles sharing edge e, with outward normal $\mathbf{n}_1, \mathbf{n}_2$, respectively. For $\mathbf{v} \in V(h)$, denote its value on T_1, T_2 by $\mathbf{v}_1, \mathbf{v}_2$. Now we examine

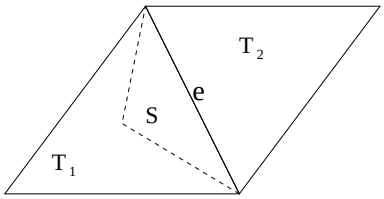

FIGURE 4. Two triangles sharing edge e with subtriangle S in T_1.

the L^2 norm of $\mathbf{v} - \gamma\mathbf{v}$ on a subtriangle S in T_1 that is associated with edge e, as shown in Figure 4. By the definition of γ,

$$\gamma\mathbf{v}|_S = \frac{1}{h_e}\int_e \frac{1}{2}(\mathbf{v}_1 + \mathbf{v}_2)\, ds = \frac{1}{h_e}\int_e (\mathbf{v}_1 - \frac{1}{2}[\![\mathbf{v}]\!]\mathbf{n}_1)\, ds.$$

Thus, by inequality (62), the triangle inequality and the Schwartz inequality,

$$\begin{aligned}
\|\mathbf{v} - \gamma\mathbf{v}\|_S^2 &\le \|\mathbf{v}_1 - \frac{1}{h_e}\int_e \mathbf{v}_1\, ds\|_S^2 + \|\frac{1}{h_e}\int_e \frac{1}{2}[\![\mathbf{v}]\!]\mathbf{n}_1\, ds\|_S^2 \\
&\lesssim h^2|\mathbf{v}|_{1,S}^2 + \frac{|S|}{4h_e^2}\left(\int_e |[\![\mathbf{v}]\!]\mathbf{n}_1|^2\, ds\right)\left(\int_e ds\right) \\
&\lesssim h^2|\mathbf{v}|_{1,S}^2 + h\|[\![\mathbf{v}]\!]\|_e^2.
\end{aligned}$$

Taking summation over all subtriangles gives inequality (19).

Next, we prove inequality (20). Consider edge e on T_1 side only. Again, since $\mathbf{v}$ has continuous normal component across e and by using inequality (18), we have

$$\begin{aligned}
\|(\mathbf{v} - \gamma\mathbf{v})\cdot\mathbf{n}\|_e^2 &= \|\mathbf{v}_1\cdot\mathbf{n}_1 - \frac{1}{h_e}\int_e \mathbf{v}_1\cdot\mathbf{n}_1\, ds\|_e^2 \\
&\lesssim h^2\|\mathbf{v}_1\cdot\mathbf{n}_1\|_{1,e}^2 \\
&\lesssim h|\mathbf{v}_1|_{1,S}^2 + h^3|\mathbf{v}_1|_{2,S}^2.
\end{aligned}$$

Sum up over all edges for all triangles in $\mathcal{T}_h$, we have inequality (20).

References

[1] D. Arnold, F. Brezzi, B. Cockburn and D. Marini, Unified analysis of discontinuous Galerkin methods for elliptic problems, *SIAM J. Numer. Anal.*, 39 (2002), 1749-1779.

[2] Douglas N. Arnold, Richard S. Falk and Ragnar Winther, *Multigrid in H*(div) *and H*(curl), Numer. Math., 85 (2000) 197–218.

[3] F. Brezzi, J. Douglas and L.D. Marini, *Two families of mixed finite elements for second order elliptic problem*, Numer. Math., 47 (1985) 217–235.

[4] F. Brezzi and M. Fortin, *Mixed and Hybrid Finite Elements*, Springer-Verlag, New York, 1991.

[5] Z. Cai, J. Mandel and S. McCormick, The finite volume element method for diffusion equations on general triangulations, *SIAM J. Numer. Anal.*, 28 (1991), 392-403.

[6] Z. Cai and S. McCormick, On the accuracy of the finite volume element method for diffusion equations on composite grids, *SIAM J. Numer. Anal.*, 27 (1990), 636-655.

[7] P. Chatzipantelidis, Finite volume methods for elliptic PDE's: a new approach, *Mathematical Modelling and Numerical Analysis*, 36 (2002), 307-324.

[8] S. H. Chou, Analysis and convergence of a covolume method for the generalized Stokes problem, *Math. Comp.* 217 (1997), 85-104.

[9] S. H. Chou and D. Y. Kwak, *A covolume method based on rotated bilinears for the generalized Stokes problem*, SIAM J. Numer. Anal., 2 (1998), 494-507.

[10] S. H. Chou and P. S. Vassilevski, *A general mixed co-volume framework for constructing conservative schemes for elliptic problems*, Math. Comp., 68 (1999), 991-1011.

[11] S. Chou and X. Ye, *Unified analysis of finite volume methods for second order elliptic problems*, SIAM Numerical Analysis, 45 (2007), 1639-1653.
[12] B. Cockburn and J. Gopalakrishnan, *Incompressible Finite Elements via Hybridization. Part I: The Stokes System in Two Space Dimensions*, SINUM 43, (2005), 1627-1650.
[13] B. Cockburn, G. Kanschat, D. Schötzau, and C. Schwab, *Local discontinuous Galerkin methods for the Stokes system*, SIAM J. Numer. Anal., 40 (2002), 319-343.
[14] M. Crouzeix and P. A. Raviart, *Conforming and nonconforming finite element methods for solving the stationary Stokes equation I*, RAIRO Anal. Numer. 7 (1973), 33-76.
[15] R. Ewing, T. Lin and Y. Lin, *On the accuracy of the finite volume element method based on piecewise linear polynomials*, SIAM J. Numer. Anal., 39, (2002), 1865-1888.
[16] R. Eymard, T. Gallouet and R. Herbin, *Finite Volume Methods, Handbook of Numerical Analysis*, Vol. VII, 713-1020. Edited by P.G. Ciarlet and J.L. Lions (North Holland), 2000.
[17] R.E. Ewing and J. Wang, *Analysis of the Schwarz algorithm for mixed finite element methods*, R.A.I.R.O. Modelisation Mathematique Analyse Numerique, 26 (1992), 739-756.
[18] R.E. Ewing and J. Wang, *Analysis of multilevel decomposition iterative methods for mixed finite element methods*, R.A.I.R.O. Mathematical Modeling and Numerical Analysis, 28 (1994), 377-398.
[19] V. Girault and P.A. Raviart, *Finite Element Methods for the Navier-Stokes Equations: Theory and Algorithms*, Springer-Verlag, Berlin, 1986.
[20] J. Huang and S. Xi, *On the finite volume element method for general self-adjoint elliptic problems*, SIAM J. Numer. Anal., 35 (1998), 1762-1774.
[21] R. H. Li, Z. Y. Chen, and W. Wu, *Generalized difference methods for differential equations*, Marcel Dekker, New York, 2000.
[22] R. Lazarov, I. Michev and P. Vassilevski, *Finite volume methods for convection-diffusion problems*, SIAM J. Numer. Anal., 33 (1996), 31-55.
[23] F. Li and C.-W. Shu, *Locally divergence-free discontinuous Galerkin methods for MHD equations* , Journal of Scientific Computing, 22-23 (2005), 413-442.
[24] R.A. Nicolaides, *Existence, Uniqueness and approximation for generalized saddle point problems*, SIAM J. Numer. Anal., 19 (1982), 349-357.
[25] J. Wang and X. Ye, *New finite element methods in computational fluid dynamics by H(div) elements*, SIAM Numerical Analysis, 45 (2007), 1269-1286.
[26] J. Wang, X. Wang and X. Ye, *Finite element methods for the Navier-Stokes equations by H(div) Elements*, Journal of Computational Mathematics, 26, (2008), 410-436.
[27] X. Ye, *On the relationship between finite volume and finite element methods applied to the Stokes equations*, Numer. Method for PDE, 17 (2001), 440-453.
[28] X. Ye, *A new discontinuous finite volume method for elliptic problems*, SIAM J. Numerical Analysis, 42 (2004), 1062-1072.
[29] X. Ye, *A discontinuous finite volume method for the Stokes problem*, SIAM J. Numerical Analysis, 44 (2006), 183-198.

Division of Mathematical Sciences, National Science Foundation, Arlington, VA 22230, USA
E-mail: jwang@nsf.gov

Department of Mathematics, Oklahoma State University, Stillwater, OK 74075, USA
E-mail: yqwang@math.okstate.edu

Department of Mathematics, University of Arkansas at Little Rock, Little Rock, AR 72204, USA
E-mail: xxye@ualr.edu